Laser and Particle Beams (1992), *vol.* 10, *no.* 4, *pp.* 617–627
Printed in the United States of America

Forward second harmonic emission from laser plasma filaments

By I. DEHA,* V. BIANCALANA, F. BIANCONI, M. BORGHESI, P. CHESSA, A. GIULIETTI, D. GIULIETTI,‡ L.A. GIZZI, L. NOCERA AND E. SCHIFANO§

Istituto di Fisica Atomica e Molecolare, Via del Giardino 7, 56127 Pisa, Italy
*Université des Sciences et de la Technologie Houari Boumedienne, Algiers,
‡Dipartimento di Fisica, Università di Pisa, Pisa, Italy, and
§Laboratoire pour l'Utilization des Lasers Intenses, École Polytechnique, Paris

(Received 10 February 1992; accepted 12 March 1992)

Experimental observations are reported on the interaction of 1-μm laser light with underdense plasmas ($n \leq 0.25\ n_c$) from thin foil plastic targets. Nominal laser intensity on target was up to 3×10^{13} W/cm^2 in a 3-ns pulse, but much higher intensity was reached due to spiky laser pulses. We studied forward-emitted second harmonic light as a diagnostic of the interaction and in particular of the occurrence of filamentation. Measurements included: energy monitoring of 2ω forward emission vs. target position and laser energy; time resolved (120-ps gate) imaging of the interaction region cross section. The second harmonic energy level was found to be sensitive to target position. In addition, the images obtained with the target in position of maximum second harmonic generation showed unstable structures whose scale length is comparable with the expected one for maximum filamentation growth. These results are shortly discussed in the framework of stationary filamentation theory and second harmonic generation in inhomogeneous media.

1. Introduction

The relevance of filamentation instability (FI) for laser fusion is well established due to its role in the interaction of laser light with coronal plasmas. FI, in fact, makes the e.m. radiation propagate into low density regions with reduced absorption. Moreover, it gives rise to strong density gradients that spoil the uniformity of the coronal plasma that surrounds the pellet. In addition, FI produces higher local intensity, which can drive several other instabilities. It is important to diagnose this instability and possibly reduce its effects.

Our group is involved in an experimental campaign in this field. Experiments are presently in progress at IFAM, Pisa, and in a larger scale in collaboration with LULI in Paris to systematically study the reliability of second harmonic (SH) emission as a diagnostic tool. At the same time, experiments have been performed at the SERC Central Laser Facility in collaboration with the Plasma Physics Group of the Imperial College, London. These latter experiments have been devoted to investigate the influence of FI on stimulated Brillouin and Raman scattering, as well as the possibility of suppressing those instabilities using beam smoothing techniques (Willi *et al.* 1990). In this article, we report on recent measurements performed in Pisa on forward-emitted SH during interaction of a 1-μm laser light with an underdense plasma.

 0263-0346/92 $5.00 + .00

Some experiments have already used SH to characterize filaments in underdense plasmas. Emission at 90° to the laser beam axis (Stamper *et al.* 1985; A. Giulietti *et al.* 1989, 1991) and in the forward direction (Meyer & Zhu 1987; D. Giulietti *et al.* 1988) has been detected in the past and related to filaments. An experiment by Young *et al.* (1989) studied SH emitted from preformed filaments and observed that only a part of the filament length contributed to the emission.

The aim of our experiment was to study the variation of SH on the position of the plasma relative to the laser beam waist and record the distribution of the SH sources. SH radiation was collected by f/4 optics and detected by means of a photomultiplier. In addition, we used a gated optical imager with a 120-ps gate time to obtain time-resolved images of the SH sources.

Details of the experimental conditions are given in Section 3. Experimental data on SH emission vs. target position and laser power, as well as time-resolved images of the interaction region in SH light, are presented in Section 4. A discussion of these results is reported in Section 5 together with some proposals for further studies on the diagnostic use of SH. The next section is devoted to some prominent features of FI and SH theory.

2. Theoretical background

Filamentation instability typically occurs when laser beam inhomogeneity causes a local depletion of plasma density in regions where laser field is higher. The consequent increase of the refractive index enhances hot-spot intensity. Diffraction and plasma internal pressure limit the growth of the instability.

Consider the electric field

$$\mathbf{E} = \mathbf{E}_0 \cos(\mathbf{k}_\perp \cdot \mathbf{r}) e^{k_\parallel z} e^{i(k_\omega z - \omega t)},$$

where the two wavevectors $\mathbf{k}_\parallel e \mathbf{k}_\perp$, which rule spatially longitudinal growth and transverse modulation, respectively, obey the law (Sodha *et al.* 1976; A. Giulietti *et al.* 1986)

$$\mathbf{k}_\parallel^2 = \frac{\mathbf{k}_\perp^2}{4\mathbf{k}_\omega^2} E_0^2 \left(\frac{\omega_p}{c}\right)^2 \left(\beta + \frac{\gamma}{\mathbf{k}_\perp^2}\right) - \frac{\mathbf{k}_\perp^4}{4\mathbf{k}_\omega^2},$$

with

$$\beta = \frac{e^2}{4m\omega^2 k_B T}, \qquad \gamma = 0.13 \left(\frac{e\nu_{ei}^2}{\omega^2 k_B T}\right)^2.$$

β and γ describe ponderomotive and thermal filamentation, respectively. This latter comes out to be negligible at high temperature and small filament scale length. Recently, Epperlein (1990, 1991) used a Fokker–Plank transport model showing that thermal filamentation can be active also at a little scale modulations. According to his scheme, the constant γ should be replaced by $\gamma' = \gamma[1 + (30 k_\perp \lambda_e)^{4/3}]$ with $\lambda_e = ((k_B T)^2 / 4\pi n e^4)$.

SH emission from filaments and, in general, due to density and intensity gradients, follows the law

$$\mathbf{J}_{2\omega} = i \frac{e^3}{4m^2\omega^3} \left(2i\mathbf{k}_\omega n(\mathbf{E}_0 \cdot \mathbf{E}_0) + n\nabla(\mathbf{E}_0 \cdot \mathbf{E}_0) + 4\mathbf{E}_0 \frac{\nabla n \cdot \mathbf{E}_0}{\epsilon}\right) e^{2i\mathbf{k}_\omega \cdot \mathbf{r}},$$

which gives the 2ω component in the current density spectrum and is obtained from Maxwell, charge continuity, and electron motion equations with negligible electronic pressure.

From SH source distribution and in infinite distance approximation one can obtain the Poynting vector

$$\mathbf{S} = \sigma \frac{\mathbf{R}}{R} \frac{L^2}{R^2\omega^4} \frac{\sin^2\chi}{\chi^2}$$
$$\times \left\{ \left[\sin^2\eta \left(A + \left(\frac{4}{\epsilon} - 1 \right) B \right)^2 + \cos^2\eta (B - A)^2 \right] \frac{\cos^2\Psi}{16} \right.$$
$$+ \left[\sin^2\eta \cos^2\eta \left(A + \left(\frac{2}{\epsilon} - 1 \right) B \right)^2 + k_\omega^2 C^2 \right] \frac{\sin^2\Psi}{4}$$
$$\left. - \left[\sin^2\eta \left(A + \left(\frac{4}{\epsilon} - 1 \right) B \right) + \cos^2\eta (B - A) \right] k_\omega C \frac{\sin\Psi\cos\Psi}{4} \right\},$$

where $\chi = [2k_\omega - k_{2\omega}\cos(\Psi)]L/2$ and σ is a factor independent from the physical parameters we shall study in the following.

In this formula, $\mathbf{R}$ is the vector from the filament to the observer, L the filament length, Ψ the azimuthal angle referred to the filament axis, and η the polar angle referred to the polarization axis of the laser incident wave (see also figure 1). Further, ϵ is the dielectric constant at ω and $k_{2\omega}$ the wavenumber of SH wave.

A, B, and C are functions given by the following integrals:

$$A = \int_0^{r_0} \frac{\partial}{\partial r} (nE^2) J_1(\tau) r \, dr$$

$$B = \int_0^{r_0} E^2 \frac{\partial n}{\partial r} J_1(\tau) r \, dr$$

$$C = \int_0^{r_0} nE^2 J_0(\tau) r \, dr,$$

with Bessel functions J_0 and J_1 calculated at $\tau = k_{2\omega} r \sin\Psi$.

Starting from these equations and for given electron density and intensity distribution of the ω light, one can study the angular emission of SH from a filament. The result depends upon the model chosen to describe filamentation and upon several parameters and we will show some calculations in Section 5. Nevertheless, some features can be pointed out here without making any assumption.

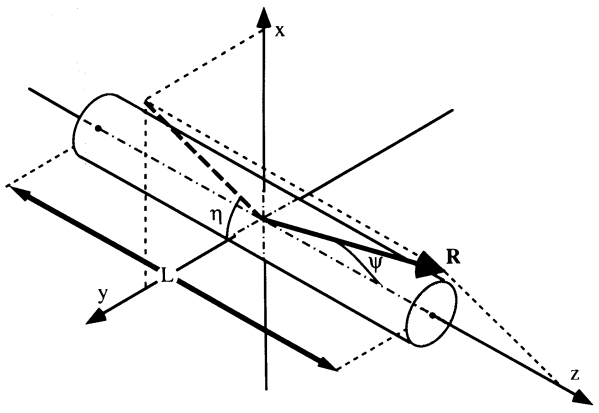

FIGURE 1. Geometry of symbols used in the Poynting vector formula. L is the length of the cylindrical filament; z is the forward direction.

Let us consider the three terms in the expression for the current density. The first is in the $\mathbf{k}_\omega$ direction, that is, parallel to the z-axis. Because this term oscillates in the direction of observation ($\Psi = 0$), no SH emission is expected on the axis. The second term has a cylindrical symmetry and points toward radial direction. Therefore, every element of the distribution has a symmetrical one with the same magnitude but phase pointing to the opposite direction. At $\Psi = 0$, these elements cancel each other so that the whole term cannot contribute to emission in the exact forward direction. The same argument applies to the third term, once again giving no SH emission in the exact forward direction.

Simple theoretical consideration can help us locate the Ψ angle of emission from an infinite length filament. From the current density equation, we know that current has a spatial phase given by the exponential factor $e^{2i\mathbf{k}_\omega \cdot \mathbf{r}}$. Because $\mathbf{k}_\omega$ is in the z-direction, this factor modulates the current along the z-axis and the emitted SH has to match with this condition. This means that the angle of emission is given by the equation $2k_\omega - k_{2\omega} \cos \Psi = 0$, i.e.,

$$\Psi = \arccos \left(\frac{1 - \dfrac{n}{n_c}}{1 - \dfrac{n}{4n_c}} \right)^{1/2} .$$

The same condition is expressed in the Poynting vector formula by the factor $L \sin^2 \chi/\chi^2$, which tends to $2\pi\, \delta(2k_\omega - k_{2\omega} \cos \Psi)$ as L goes to infinity. For finite filament length, the function $L \sin^2 \chi/\chi^2$ contributes to SH emission at smaller angles as far as L becomes shorter.

Finally, we have to take into account the term in braces in the Poynting vector expression, which depends upon electron density and local laser intensity. This can make, for certain choices of parameters and distributions, emission predominant at angles other than the maximum of the function $L \sin^2 \chi/\chi^2$.

3. Experimental conditions

The 3-ns, 2.51-J laser pulse generated by a neodymium laser ($\lambda = 1.064\ \mu$m) was made up of approximately half a dozen intense spikes of $\approx$50-ps duration.

A small fraction of the laser beam was used to control pulse energy and shape. An f/8 lens focused the beam on target in a vacuum chamber. The focal spot was 60 μm in diameter and the nominal intensity was up to 3×10^{13} W/cm^2. The peak intensity for each spike can be roughly estimated 10 times higher than the nominal intensity so that a maximum intensity up to 3×10^{14} W/cm^2 has to be considered when dealing with effects developing in a short time scale.

The plasma was produced by irradiating 1-μm thick plastic foils ($Z = 3.2$, $A = 5.7$) placed in the beam waist. In this condition, at the peak of the pulse a plasma density of $n \leq 0.25\ n_c$ and a temperature of $T \approx 500$ eV has been measured in previous experiments (D. Giulietti *et al.* 1991). The forward-emitted light was collected by an f/4 lens. Multilayer interference mirrors and filters were used as sketched in figure 2 to select a 30-Å spectral window around 5,320 Å.

SH energy measurements were performed using a photomultiplier whose signal was recorded by a storage oscilloscope. Time-resolved images of the SH sources emitting forward were obtained by means of a gated optical imager (GOI) used alternatively to the photomultiplier to avoid possible optical disturbances introduced by the beam splitter (item 7 in figure 2). The GOI output was recorded on HP5 films. GOI is an optoelectronic device

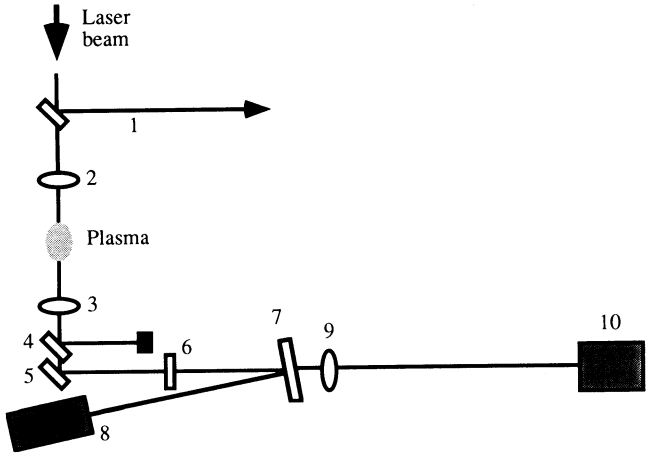

FIGURE 2. Experimental setup. A small fraction of the laser beam is sent to beam diagnosis line 1. The laser beam is focused by lens 2 on a thin plastic foil. Lens 3 collects the outcoming light. The interference mirror 4 reflects laser light away to a dumper; then, the interference mirror 5 selects SH. The narrow band (30 Å) interference filter 6 completes spectral selection. Energy measurements were obtained with photomultiplier 8, and lens 9 imaged out the plasma on the photocathode of the gated optical imager 10.

based upon an 18-mm wide S25 photocathode coupled to a microchannel plate. The optical magnification at the input plane of the GOI was 80, which, taking into account the 10 lines/mm resolution of the GOI, allows $\approx$1-μm details to be resolved in the plasma, comparable with the 2-μm diffraction limit. The optical intensifier was electronically gated with a 120-ps pulse synchronized approximately at the peak of the 3-ns laser pulse.

4. Experimental results

We measured forward-emitted SH energy vs. target position, which revealed an interesting behavior as evidenced in figure 3.

In this plot, a strong variation of SH emission is shown for relatively small target displacements. At the maximum level of laser energy, an increase of more than two orders of magnitude in SH emission resulted from target displacements of 0.2 mm (small if we consider that the measured focal depth is about 0.6 mm).

At 10 times lower incident laser energy, the effect is still evident, while it disappears when the energy is reduced below 0.1 J. Actually, the low emission detected when the target is definitely out of focus or at low laser energy levels is not to be attributed to SH but to bremsstrahlung emission. This was simply verified by tilting the interferential filter (item 6 in figure 2), so shifting the allowed spectral region of several tens of Å. In this condition, signals obtained with the target out of focus or at low laser energy remained unchanged despite what one should expect if they were second harmonic. On the contrary, the filter tilt strongly reduced signals obtained with the target near the focus and at higher laser energy.

A scan of SH energy vs. incident laser energy at three target positions was also performed and results are shown in figure 4. Different slopes can be attributed to the three target positions. At the position of maximum SH emission, a nearly cubic (power 2.8) law resulted. A 1-mm defocusing produced a nearly quadratical behavior (power 1.8). A sublinear dependence is obtained 1.5 mm away from the position of maximum emission. Notice that

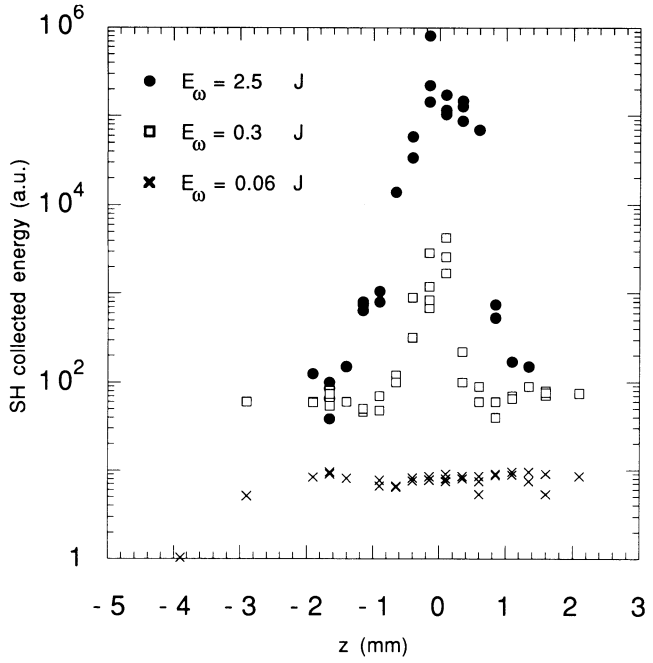

FIGURE 3. SH energy as a function of target position at three different levels of incident energy. SH emission varied more than two orders of magnitude by displacing the target of 0.2 mm. The laser beam comes from negative values of z.

at energy below 0.1 J, where the three curves converge, the signal is simply due to bremsstrahlung self-emission of the plasma.

A first attempt to know the angular distribution of the forward-emitted SH was done by putting diaphragms of different apertures in front of the collecting lens 3 (see figure 2). We observed that most of the SH collected by the lens was included in a cone of total aperture $\approx 10°$.

The structure of SH sources at the peak of the pulse was investigated by taking time-resolved images with the GOI. The light was spectrally selected in a 30-Å bandwidth as for energy measurements. The images were taken at two different target positions and maximum laser energy. An experimental problem was the shot by shot intensity variation on the GOI photocathode due to the timing of the electronic gate relative to SH spikes. A fluctuation in intensity of about one order of magnitude was observed, resulting in some cases in saturated or weak images.

Most of the images taken with the target in the position of maximum SH emission were characterized by a bright 30-μm nucleus broken in several structures less than 10 μm in size. Moreover, weak fringes were visible around this central region. The detailed pattern of the SH sources varied shot by shot. A typical image obtained with target in the maximum SH emission is shown in figure 5.

With the target 1 mm before the focus, a dramatic decrease in SH intensity reaching the GOI photocathode was observed, in agreement with data plotted in figure 4. Nevertheless, several good-quality images were obtained, showing a completely different distribution of the SH sources, as shown in figure 6. The main structure was stable shot by shot and consisted of two 15-μm sources at a distance of 30–40 μm along a given axis. Some fringes were on occasion visible around the separated nuclei.

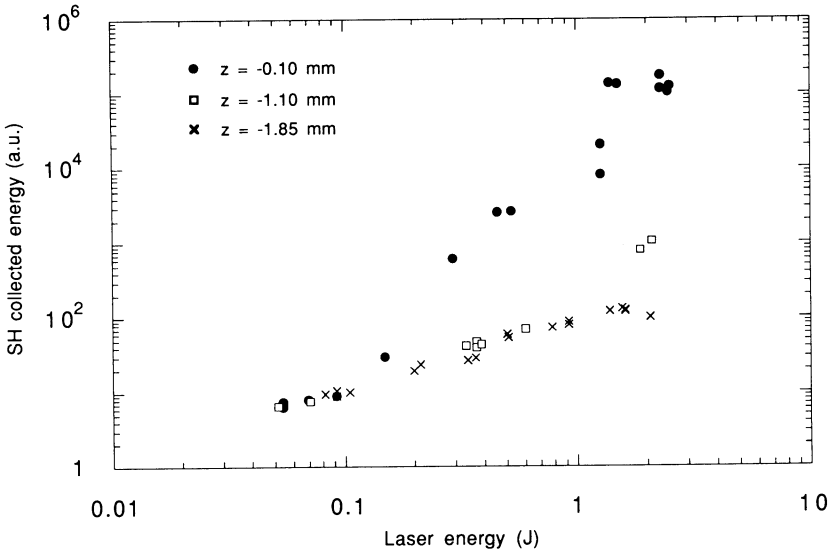

FIGURE 4. SH vs. incident laser energy. Measurements were performed with three target positions ranging within 1.75 mm.

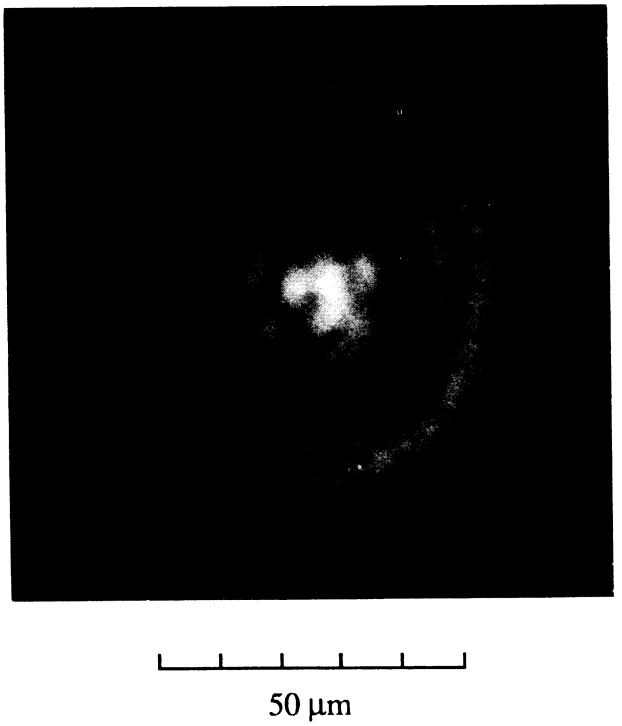

FIGURE 5. Image of SH sources taken with the target in the maximum SH power position: 120-ps gate at the peak of the laser pulse. Nominal intensity on target: 3×10^{13} W/cm^2.

FIGURE 6. Image taken with target 1 mm away from the position of maximum SH production toward the laser. Other conditions as for Figure 5. The SH intensity reaching the GOI cathode was about 500 less than in the case of Figure 5.

5. Discussion

Energy measurements clearly show that forward-emitted SH is extremely sensitive to changes in the interaction condition. This is in particular evident for the "geometry" of the interaction, i.e., the relative position of beam waist and plasma density profile of the exploding foil. At full laser power, SH experiences variations in energy of three orders of magnitude above the continuum background for target displacements of the order of the depth of focus. Reciprocally, in the position of maximum emission SH depends definitely more than quadratically upon the laser pulse energy. This behavior smooths out progressively when the target is moved away form the focus and/or laser energy is reduced.

If we exclude data obtained at laser energy below 0.1 J, for which plasma self-emission dominates, SH vs. laser energy data are surprisingly well fitted by power laws, the exponent changing regularly with target position. However, it is difficult to model this behavior because plasma parameters change with laser pulse energy.

On the other hand, the dramatic effect of target position on SH emission cannot be reasonably attributed to the variation of the average laser intensity on target, which would be small in the absence of nonlinear phenomena. Figure 3 evidences that starting from some target positions a displacement of 0.2 mm causes SH energy to jump up by two orders of magnitude. Such a displacement is definitely smaller than the focal depth (0.6 mm) we measured for the focused beam. This fact proves that a nonlinear part of the refraction index is induced in the plasma by self-focusing and filamentation in such a way that an "extra lens" is activated.

Self-focusing and filamentation are directly shown by time-resolved images obtained in SH light. With the target in position of maximum SH emission, there is evidence that the beam diameter collapses from 60 to about 30 μm. At the same time, unstable structures appear of less than 10 μm in size. We studied separately several different planes inside and outside the depth of focus by the equivalent plane method and were not able to find similar structures in the laser beam cross section. Moreover, we found that the beam profile remains stable shot by shot, while SH sources do not.

With the target 1 mm away from the position of maximum emission, SH sources are distributed differently and their distribution is highly reproducible shot by shot. This fact, as well as a comparison with the beam spot shape slightly out of the best focus, suggests that in this case the SH emitting gradients are heavily influenced by the original intensity distribution in the beam rather than by filamentation instability. On the contrary, this latter seems to dominate the interaction when high SH emission occurs.

In this respect, it is interesting to compare the size of the observed SH small spots, as in figure 5, with the ordinary theory of FI. The transverse modulation for maximum growth of the instability referred to our experimental condition has been calculated for two densities, $n_c/4$ and $n_c/8$. The first is expected to be the maximum intensity of the exploding foil plasma at the peak of the pulse, as also observed from $3\omega/2$ measurements (D. Giulietti *et al.* 1991). If we simply assume that the transverse modulation wavelength is twice the filament diameter d, we find $d \approx 7$ μm at $n_c/4$ and $d \approx 11$ μm at $n_c/8$. Comparing these approximate values with diameters we measured in time-resolved images (<10 μm), we could infer that FI occurred in a plasma region whose density was between those two limits.

Let us now briefly calculate the angular distribution of SH energy starting from the Poynting vector as given in Section 2. We put for electron density and field distributions

$$n = n_0 e^{-\alpha[1-(r/r_0)]^2}$$

$$E^2 = E_0^2\left(1 - \frac{r}{r_0}\right)^2,$$

which provide mechanical equilibrium between ponderomotive and plasma pressure when

$$\alpha = \frac{4\pi e^2 E_0^2}{2mk_B T\omega^2}.$$

For the internal field E_0, we took the average value along the filament

$$E_0 = E_{in}\frac{e^{k_\parallel L} - 1}{k_\parallel L}.$$

The intensity at the filament "entrance" was equated to the peak value for a single spike in the pulse, namely, 3×10^{14} W/cm^2. Electron plasma temperature was put equal to 500 eV. The result of the calculation gives the SH power collected in a solid angle of half aperture Ψ. In figure 7, curve (a) refers to filaments generated at $n_c/8$, 150 μm in length, 11 μm in diameter. The filament diameter is the one of maximum growth and the filament length is the corresponding growth length. Similarly, curve (b) refers to filaments generated at $n_c/4$, 60 μm in length, 7 μm in diameter. The dotted vertical line in the diagram of figure 7 shows the aperture of our collecting optics. The most relevant features of both curves are: (1) the lack of SH emission close to the forward direction up to 2 and 5° in cases (a) and (b), respectively; (2) a virtual lack of SH emission at angles larger than 8 and 12°, respectively; (3) a definite step of SH emission for each curve at Ψ_1 and Ψ_2, respectively. Ψ_1 and Ψ_2 are the angles of best-phase matching, where $\chi = 0$ in the factor $L \sin^2 \chi/\chi^2$ of the Poynting vector from Section 2. These features can be used as complementary diagnos-

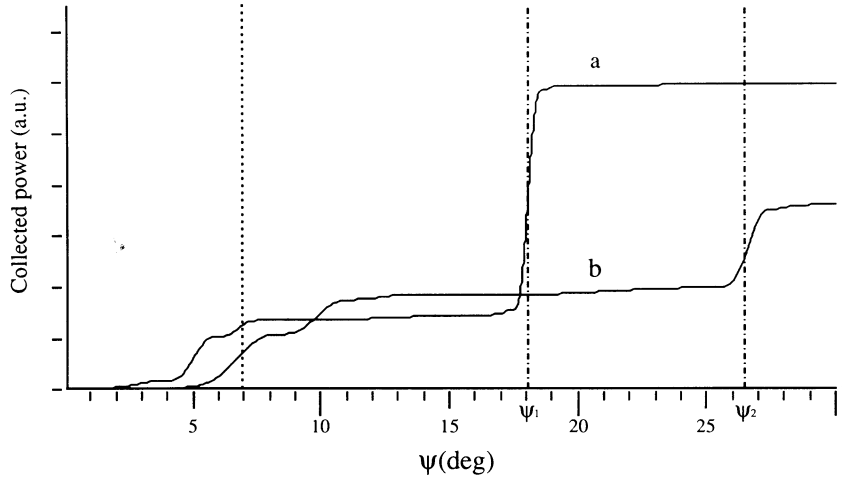

FIGURE 7. Collected SH power vs. Ψ: Theoretical plot for two filaments. Curve (a) corresponds to the best-growing filament at $n = n_c/8$ with 150-μm length and curve (b) to the best-growing filament at $n = n_c/4$ with 60-μm length.

tics of filamentary plasmas if SH angular distribution is known. In particular, if the large angle step is evidenced this should mean that filaments are preferentially generated at a given density. Unfortunately, in our measurements the aperture of our collecting optics was not large enough to scan over these values of Ψ. The preliminary rough measurements of the angular distribution up to $\Psi = 7°$ suggest that filament parameters are closer to those of curve (a) rather than (b). Of course, better angular distribution measurements are needed, as well as a more accurate modeling of the process.

6. Conclusion

Forward-emitted second harmonic provides a powerful diagnostic tool for the study of gradients induced by nonlinear interaction of laser light with underdense plasmas. Both energy measurements and time-resolved imaging are suitable to this purpose. Our second harmonic measurements gave information on filamentation instability that would be difficult to achieve otherwise. Variations of orders of magnitude have been observed in the second harmonic level for small displacements of the plasma with respect to the beam waist. Filaments have been evidenced whose size is comparable with the one expected for the maximum growth of filamentation instability.

Acknowledgments

The authors are grateful to the Plasma Physics Group, Imperial College, London, which supplied them with the GOI device, and in particular to Oswald Willi, who also participated in part of the measurements. They also mention Dimitri Batani for his initial contribution. One of us (I.D.) is indebted to the International Centre for Theoretical Physics, Trieste, for its grant support.

REFERENCES

EPPERLEIN, E.M. 1990 *Phys. Rev. Lett.* **65**, 2145.

EPPERLEIN, E.M. 1991 *Phys. Fluids B* **3**, 3082.

GIULIETTI, A. *et al.* 1986 In *Laser Interaction and Related Plasma Phenomena, Vol. 7*, p. 259. H. Hora and G.H. Miley, eds. (Plenum, New York).

GIULIETTI, A. *et al.* 1989 *Phys. Rev. Lett.* **63**, 524.

GIULIETTI, A. *et al.* 1991 In *Laser Interaction and Related Plasma Phenomena*, Vol. 9, p. 273. H. Hora and G.H. Miley, eds. (Plenum, New York).

GIULIETTI, D. *et al.* 1988 *Laser Particle Beams* **6**, 141.

GIULIETTI, D. *et al.* 1991 *Nuovo Cimento* **13D**, 845.

MEYER, J. & ZHU, Y. 1987 *Phys. Fluids* **30**, 890.

SODHA, M.S. *et al.* 1976 *Progress in Optics, Vol. 13* (Academic Press, New York).

STAMPER, J.A. *et al.* 1985 *Phys. Fluids* **28**, 2563.

WILLI, O. *et al.* 1990 *Phys. Fluids B* **2**, 1318.

YOUNG, P.E. *et al.* 1989 *Phys. Rev. Lett.* **63**, 2812.